# AI-Based Wireless Cardio-Pulmonary Stethoscope for Continuous Non-Invasive Assessment of Lung Water Status

Christopher Leong, *Student Member, IEEE*, Yuanzhang Xiao, *Member, IEEE*, Zhengqing Yun, *Senior Member, IEEE*, and Magdy Iskander, *Fellow, IEEE*

***Abstract*— *Objective:* Early detection of excessive lung water is vital to keep patients from deteriorating into critical conditions such as heart failure. Previously, we developed a non-invasive wireless cardio-pulmonary stethoscope (CPS) that effectively estimates the change of lung water content and vital signs (e.g., heart rates, respiratory rates) in a clinical trial funded by National Institutes of Health (NIH). In this work, the capability of the CPS is expanded to assess lung water status (i.e., normal, moderate edema, and edema), in addition to the change of lung water. *Methods:* First, we identify an NIH database containing lung images of a diverse population. An automatic workflow is proposed to convert these images to 3D lung objects in High-Frequency Simulation Software and obtain the S-parameters of the lungs at different water levels. Next, we develop a personalized machine learning model to assess lung water status based on patient attributes and S-parameter measurements. Decision trees are chosen as our models for the superior accuracy and interpretability. Important patient attributes are identified for lung water assessment. A "cluster-then-predict" approach is adopted, where we cluster the patients based on their ages and fat thickness and train a decision tree for each cluster, resulting in simpler and more interpretable decision trees with improved accuracy. *Results:* Our models achieve more than 70% accuracy in assessing lung water status of 103 male and 101 female patients. *Conclusion and Significance:* Our proposed method enables continuous and non-invasive assessment of the lung water status for a diverse population of patients.**

***Index Terms*— Artificial intelligence, lung water, non-invasive, wireless cardio-pulmonary stethoscope**

## I. Introduction

CHRONIC heart failure, pulmonary hypertension, acute respiratory disorder syndrome (ARDS), and kidney failure and their acute exacerbations are among the leading causes of hospitalization, health care costs, and deaths in the United States. For example, more than one million patients are hospitalized annually due to heart failure, which accounts for a total medicare expenditure exceeding $17 billion. In multiple disease states, through injury or pressure or both, these protective mechanisms fail, resulting in the abnormal accumulation of extravascular lung water. Hence, close monitoring of lung water status, respiratory rates and heart rates is key to proactively preventing the worsening of patient heart failure and treating acute exacerbations. For instance, the assessment of a patient with left ventricular systolic dysfunction and progressive dyspnea includes an evaluation of volume status and extravascular lung water – often assessed by measuring weight, jugular venous pressure, and presence of an S3 on cardiac exam, or peripheral edema. Similarly, patients with symptomatic hypotension are often assessed for their volume status, particularly if dehydration is a consideration and/or when complicating factors (e.g., renal insufficiency, peripheral neuropathy, and concomitant comorbid illnesses) confound the diagnostic exam. In summary, early detection of excess lung water is critical to provide timely fluid assessment and improve treatment for patients with chronic diseases such as heart failure.

However, existing modalities of monitoring lung water are either costly (e.g., chest X-ray and computerized tomography (CT) scan) and/or invasive (e.g., cardiac catheterization), making them unsuitable for continuous monitoring and early detection of excessive lung water. Therefore, we have developed a wireless cardio-pulmonary stethoscope (CPS) to continuously monitor the change of lung water content and other vital signs (e.g., heart rates, respiratory rates) [1]–[4]. The proposed CPS consists of small sensors that can be conveniently attached to the patient's chest and a smart device that receives the measurements from the sensor and displays the change of the lung water content along with other vital signs such as heart rates and respiratory rates [5].

The continuous non-invasive monitoring capability of the proposed CPS is achieved by using highly penetrating radio frequency (RF) and electromagnetic waves. At microwave frequencies, the dielectric properties of lung tissues are closely related to the water content in the lungs, as discovered and validated by our prior works through simulations [6], phantoms [7], and animal experiments [8]. Our prior efforts of clinical trials have demonstrated that the CPS can accurately detect the change in lung water content [2].

In this work, we propose an artificial intelligent (AI) based lung water prediction to significantly expand the capability of our wireless CPS. First, we aim to assess the lung water

This work was supported in part by the U.S. National Science Foundation under Grant 1822213.

The authors are with Hawaii Advanced Wireless Technologies Institute at the University of Hawaii, Manoa, Honolulu, HI, USA (correspondence e-mail: magdy.iskander@gmail.com).

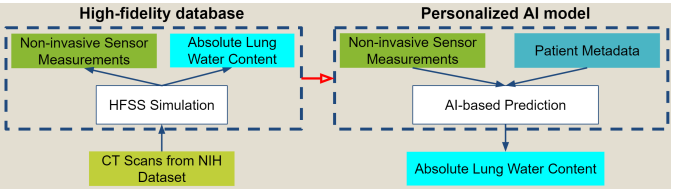


Fig. 1. The proposed framework of AI based lung water assessment.

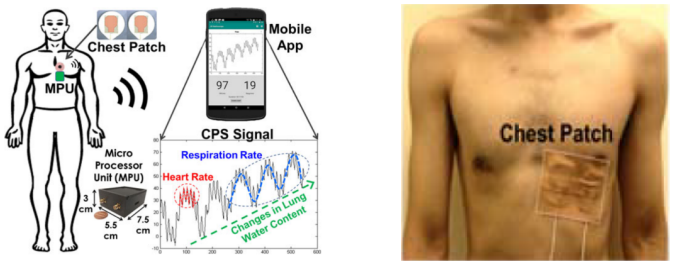


(a) Wireless CPS (b) Chest patches

Fig. 2. Illustration of the wireless CPS and chest patches.


Fig. 3. Left: Setup for SAR experiments and RF-safety evaluation of the CPS system. Right: CPS results are significantly lower than commercially available mobile devices and is one fourth of the FCC SAR safety limit.

status (i.e., normal, moderate edema, and edema), in addition to the change of lung water. Second, we seek to build accurate personalized AI models for diverse patient populations. One key challenge to develop a personalized AI model is to build a database of a diverse patient population, because individuals are different both in the baseline dielectric property of normal lung tissues and in the changes of dielectric properties under different severities of edema. The high cost of collecting data from clinical trials makes the challenge even more difficult. To address this challenge, we use a large NIH data set of CT scan images, and develop an automatic workflow to obtain high-fidelity data from 3D high-frequency simulation software (HFSS). This generates a data set that includes patients with varying ages, genders, and sizes, and the scattering parameters (S-parameters)[1] of their lung tissues under various amounts of lung water. Compared to collecting data from clinical trials, our approach is low-cost, less time-consuming, and risk-free.

Based on the data set built, we propose highly accurate and interpretable machine learning models for personalized assessment of lung water status. We first compare different classifiers and choose the decision tree classifier for its superior accuracy and interpretability. We then identify important features, namely S-parameters, genders, ages, and thickness of fat layers, for lung water assessment. Finally, we adopt a cluster-then-predict approach, where we cluster the patients into subgroups based on their genders, ages and fat thickness and train decision trees for each subgroup. This approach further improves the interpretability and accuracy of the decision trees for each subgroup. The final decision trees for each subgroup determine the lung water status using the magnitudes and the phases of the S-parameters only. On average, our personalized models achieve higher than 70% accuracy of lung water status assessment over a diverse group of 103 male and 101 female patients. The proposed framework is illustrated in Fig. 1.

A preliminary version of this work has been reported [9]. The current work significantly expands our prior work [9] by describing the automatic workflow of building the database in detail (Section III) and including the development of the AI models (Section IV).

The rest of the paper is organized as follows. Section II reviews the wireless CPS system. Section III describes the automatic workflow to build the database from a large NIH data set. Section IV delineates the development of the personalized machine learning models for lung water status assessment. Finally, Section V concludes the paper.

[1]S-parameter is the measure of the magnitude and phase of the received signal by the non-radiating sensor, as a result of the scattered radio frequency (RF) signal inside the patient body.

## II. Overview of The Proposed Wireless Cardio-Pulmonary Stethoscope

At radio frequencies (RF), the dielectric properties of lung tissues are closely related to the amount of water content in the lungs. Based on this principle, we have developed the wireless CPS device and measurement methods for continuous monitoring of RF scattering parameters (reflection/transmission coefficients) and extracting lung water, heart rate, and respiration rate from a single measurement. As illustrated in Fig. 2, the CPS system consists of an adhesive chest patch containing two electrocardiogram (EKG) lead sized RF sensors and measurement hardware and data analysis software components. The patch is placed in contact with the patient's chest, scattering parameters are measured at 915 MHz, and multiple vital signs are derived from a single measurement using digital signal processing algorithm. As demonstrated in animal experiments and clinical evaluations, the CPS accurately measures changes in lung water content and monitor the heart rate and the respiration rate in real time and in a noninvasive manner.

The CPS is also safe. The industry standard for RF safety evaluation of electromagnetic devices is specific absorption rate (SAR), which quantifies the rate at which energy is absorbed per unit mass in an exposed object [10]. SAR values of our device were measured at the Federal Communications Commission (FCC) Safety Compliance Facility and compared with SAR values for several commercially available mobile phones. As shown in Fig. 3, the SAR value of the CPS is only one fourth of the FCC's RF safety standard limit, and is lower than any of the most popular mobile brands.

The developed CPS system was recently tested on heart failure and hemodialysis patients. Results from clinical trials with heart failure and dialysis patients showed excellent correlations with other available clinical monitoring methods

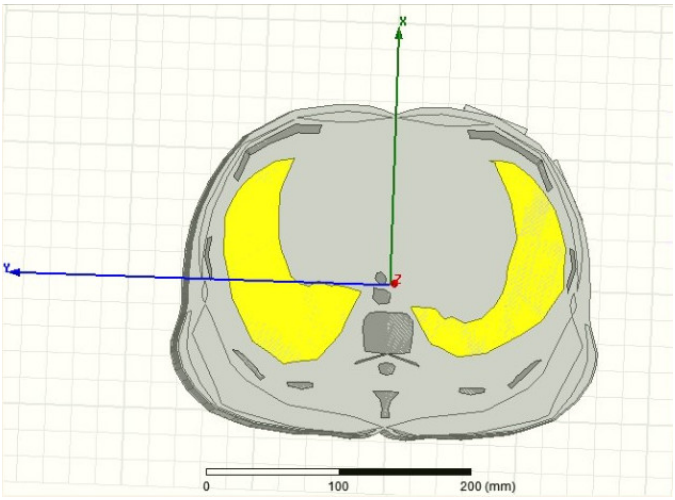


Fig. 4. Axial cross-section of human body at the height of sensor attachment. Yellow polygons represent lungs, dark gray polygons represent bones, and gray polygons represent an averaged mixture of epithelial, muscle, and fat tissues.

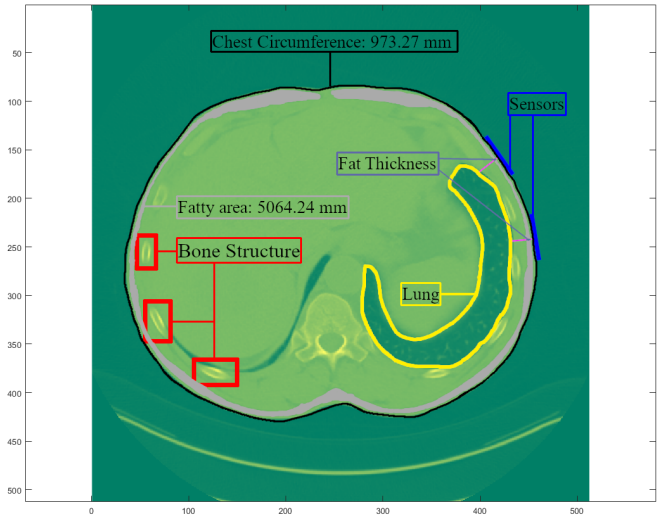


Fig. 5. Axial cross-section at the height of the CPS sensor in MATLAB. Dark gray structures are bones of the thoracic cage while those in yellow are lung tissues. The sensors are attached at the top-right of the body. We use the chest circumference and the fat thickness, which can be measured conveniently, as features for the machine learning models developed next.

[2]. Specifically, results from clinical trials showed that heart and respiration rates of all patients have correlation factors higher than 0.9. Comparisons with fluid removed during hemodialysis treatment showed correlation factors of 0.82 to 1, while comparisons with pulmonary capillary wedge pressure measurements for heart failure patients had correlation factors of 0.52 to 0.97.

## III. Building The Database Based on a Large-Scale NIH Dataset

To address the challenges of the lack of data and the high cost of collecting data from clinical trials, we develop a automatic workflow to build the database from a large-scale NIH dataset, DeepLesion [11]. DeepLesion contains thousands

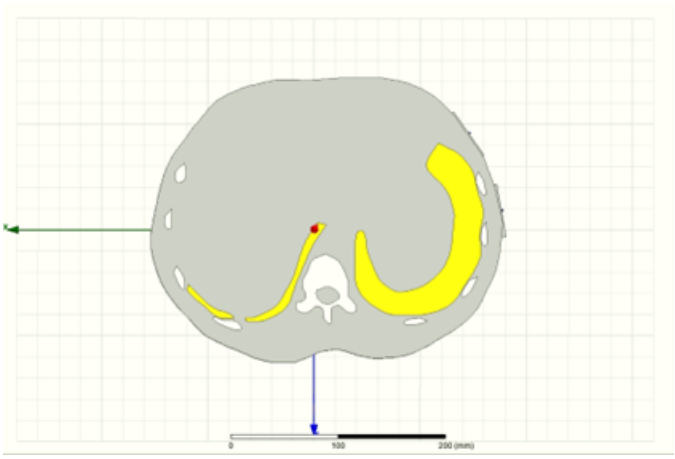

Fig. 6. The cylindrical model built from the axial CT scan in HFSS. A 3D model of the sensor is attached to the body (adjacent to the cylinder) at the middle height of the cylinder. Yellow polygons represent lungs, white polygons represent bones, and gray polygons represent an averaged mixture of epithelial, muscle, and fat tissues.

TABLE I
DIELECTRIC PROPERTIES USED FOR THE LUNG POLYGONS, BASED ON FRACTIONAL VOLUMES OF BLOOD, AIR, AND LUNG TISSUE [12].

| Lung Water Content | Relative Permittivity | Electrical Conductivity (S/m) |
|---|---|---|
| 20% | 20.604 | 0.417 |
| 40% | 30.679 | 0.590 |
| 60% | 40.510 | 0.755 |

of axial CT scans. An axial CT scan provides a cross-section with respect to height. For modeling and simulation purposes, the scans provide detailed positions and shapes of the lungs and bone structures with respect to their body's overall chest shape. Previous simulations using the CPS model would scan a human body model at the cross-section, shown in Fig. 4 with located bone structures and lungs. CT scans are chosen based on their similarity to the cross-section. It is assumed that its locations are similar with respect to height. Some CT scans are disregarded because the lung is not present due to the respiratory cycle.

We use MATLAB to import a CT scan and detect the edges of the chest, bone structures, and lungs (see Fig. 5). The CT scans are 512 by 512 pixel images. DeepLesion provides the pixel to mm conversion, ensuring that we have the correct sizes. The polygons composed of these edges are written into a script. HFSS use these polygons to build a cylindrical model of the lung. Each CT scan represents a patient, and the gender, the age, the thoracic circumference, the fatty area, and fat layer thickness are recorded in the database.

Simulation of the CT scan's cylindrical model is performed in Ansys HFSS [13]. HFSS is an electromagnetic solver and can be used to determine the S-parameters for a given structure at given frequencies. The script from MATLAB is imported into HFSS to create a cylindrical model (see Fig. 6). Two CPS sensors are attached at the middle height of the cylinder and at locations with a clear view of the lung (i.e., no blockage by bone structures). The exact locations are determined by a MATLAB script based on the cross-section outline. The two

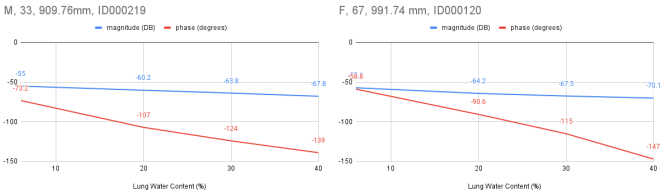


(a) 33-year-old male (b) 67-year-old female

Fig. 7. Sample results of HFSS simulation for a 33-year-old male and a 67-year-old female. We obtain magnitudes and phases of S-parameters at different lung water levels.

sensors are placed 8cm apart to increase the likelihood of avoiding the thoracic cage. The simulation is performed at lung water content of 20% (normal lung water), 40% (moderate edema), and 60% (edema) at 915MHz, by changing the lung polygon's dielectric properties. The properties used for each lung water state are shown in Table I. The dielectric properties are based on fractional volumes as the lung can be considered homogeneous near microwave wavelengths [12]. Magnitudes and phases of the S-parameters are taken for the lung water content of each patient. Fig. 7 shows the S-parameters at different lung water levels for two representative patients.

## IV. AI-Based Lung Water Assessment

We aim to assess the lung water status based on the patient attributes (i.e., gender, age, chest circumference, fat thickness) and S-parameters (i.e., magnitudes and phases). We pose the problem as a classification problem with three classes, namely *normal* (i.e., 20% lung water content), *moderate edema* (i.e., 40% lung water content), and *edema* (i.e., 60% lung water content). We have data samples of 103 male patients and 101 female patients with ages from 20 to 86.

### A. AI Model Selection

There are a variety of models available to perform the classification task. Our first step is to select the model that is most suitable for our data based on accuracy and interpretability. We consider the following commonly-used classification models.

- Support vector machines (SVM) [14]: SVM maps the input vectors non-linearly to a high-dimension feature space, and then uses linear decision surfaces in the feature space to separate the data samples. We evaluate linear SVM (which removes the non-linear mapping) and radial basis function (RBF) SVM (which uses the radian basis function as the non-linear mapping).
- Decision trees [15]: A decision tree classifier uses "if-then" type decision rules on the features to predict the class of a data sample. A decision tree can be seen as a piece-wise constant approximation.
- Random forests [16]: A random forest classifier is the average of multiple decision tree classifiers.
- Neural networks [17]: A neural network is a network of neurons (i.e., simple processing units specified by an activation function). A neural network can implement highly non-linear classification rules by adjusting the connections between the neurons.
- Nearest neighbors [18]: A nearest neighbor classifier groups the training samples "closest in distance" to the new point, and predict the class from these samples. A nearest neighbor classifier can also be highly non-linear.

Fig. 8 illustrates the data samples for all the male patients and the decision regions and classification accuracy of the above AI models.

From the plot of the data samples, we can see that the data cannot be separated by straight lines. Therefore, linear models, such as linear SVM, are not accurate. Based on this observation, we focus on commonly-used nonlinear models, namely RBF SVM, decision trees, random forests, neural networks, and nearest neighbors. Among all the non-linear models, nearest neighbors have the highest accuracy. However, the decision regions of the nearest neighbors are too complex to explain. We observe that decision trees have same or higher accuracy than RBF SVM and neural networks. Compared to random forests, decision trees have slightly lower accuracy, but much simpler decision regions. Overall, we found that decision trees have the best accuracy and interpretability trade-off.

Another advantage of decision trees is that the decision rules have the if-then structure that resembles natural language and the way humans think (see Fig. 9 for an illustration of the decision tree). For example, the decision tree in Fig. 8 stipulates the following decision rule: If the phase is between -167.5 and -133.5 and the magnitude is above -64.7 dB, the lung is normal; if the phase is between -167.5 and -133.5 and the magnitude is below -64.7 dB, the lung has moderate edema; if the phase is between -177.5 and -172.5, the lung has moderate edema; otherwise, the lung has edema. We can see that decision trees provide human-friendly explanations, which is especially desirable in clinical settings.

### B. Feature Selection

Now that we have decided to use decision trees as our model, we proceed to perform feature selection. Our goal is to select the most important features, instead of using all the features, for the model. Feature selection will improve the model generalizability and interpretability [19].

There are different methods to quantify feature importance. We use the permutation importance, a metric commonly used in practice, to measure the importance of each feature [19], [20]. Permutation importance measures the impact of a feature on the classification accuracy. Specifically, to evaluate a feature, we create data sets with random permutations of the feature to evaluate while keeping the other features the same, and see how much the classification accuracy drops. When permuted, a more important feature will result in a larger drop in the accuracy.

Fig. 10 shows the permutation importance of several decision trees with different tree depths. We can see that the phase is by far the important feature. The magnitude and the fat thickness are the next two important features, with the relative importance of these two varying across models. The circumference and the age are the least important.

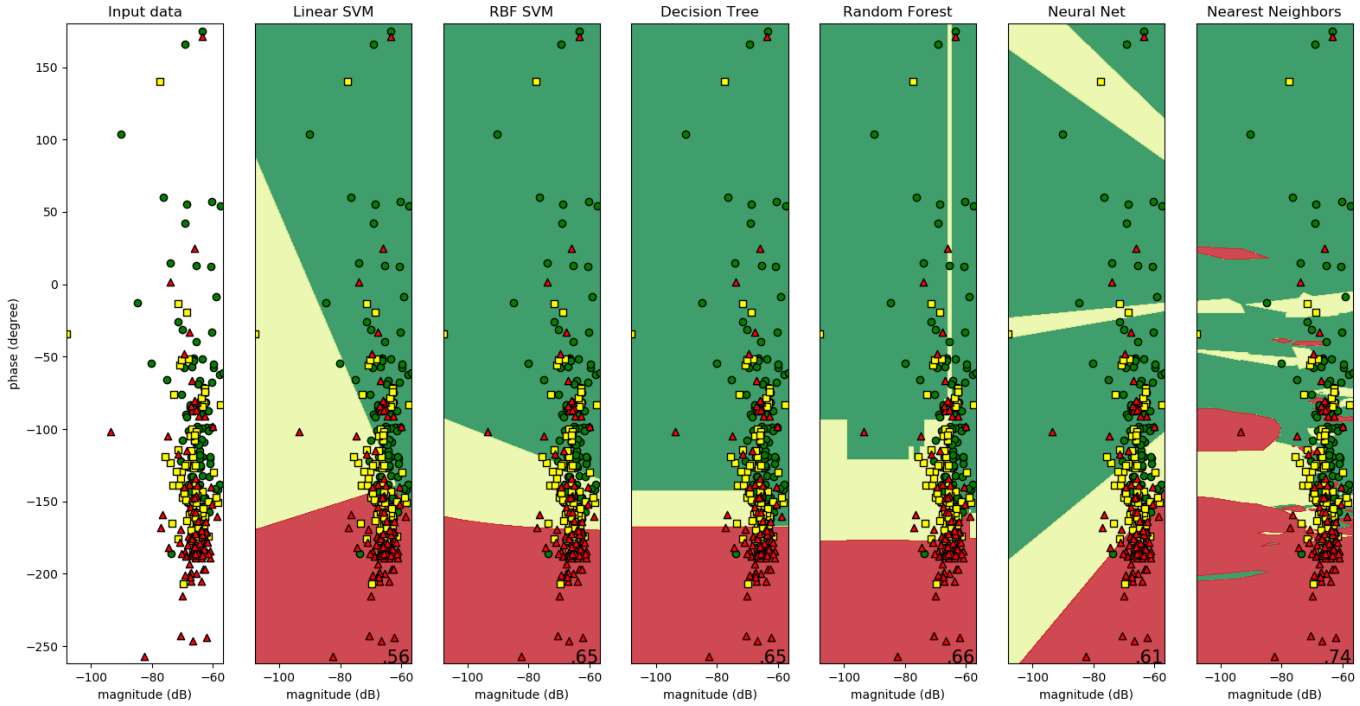


Fig. 8. Illustration of data samples and decision regions of different machine learning models. In all the subplots, the x-axis and y-axis are the magnitude and the phase of the S-parameters, and the green circles, yellow squares, and red triangles are the data samples representing normal lung water (20%), moderate edema (40%), and edema (60%), respectively. Leftmost: the data samples; Right: decision regions of nearest neighbors, decision trees, random forests, and neural networks, respectively, where green, yellow, and red pixels indicate that the model classifies the corresponding samples as normal lung water, moderate edema, and edema.

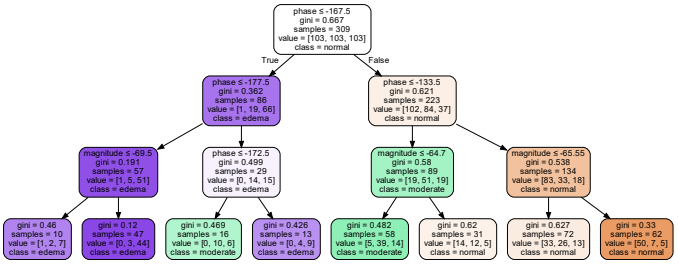


Fig. 9. Illustration of the decision rules stipulated by the decision tree classifier in Fig. 8: If the phase is between -167.5 and -133.5 and the magnitude is above -64.7 dB, the lung is normal; if the phase is between -167.5 and -133.5 and the magnitude is below -64.7 dB, the lung has moderate edema; if the phase is between -177.5 and -172.5, the lung has moderate edema; otherwise, the lung has edema.

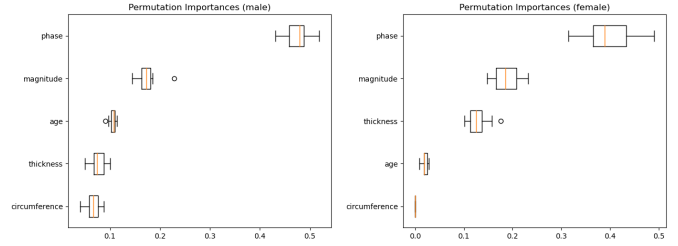


(a) male patients (b) female patients

Fig. 10. Illustration of the permutation importance of all the features for decision trees. For each feature, the box plot shows the median of the importance (the orange line), the first and the third quartiles (the box), 1.5 times the interquartile range (IQR) beyond the third quantiles (the whiskers extending from the box), and the outliers (the circles).

### C. The Cluster-Then-Predict Approach

Based on the important features identified, we adopt the cluster-then-predict approach to build the final AI models [21], [22]. Specifically, we first cluster the patients into subgroups, and then train a decision tree classifier for each subgroup of patients. The advantages of the cluster-then-predict approach are higher average accuracy due to the similarity of patients within one subgroup and better interpretability due to simpler classifiers for each subgroup.

We first determine the features that serve as the basis to cluster the patients. It is important to use features that are constant (i.e., age, circumference, and fat thickness) for clustering. If we were to use time-varying features (e.g., magnitude and phase) for clustering, the subgroups would change quickly over time. Based on the feature importance shown in Fig. 10, we drop the circumference as a feature due to its low importance. We first try to cluster the patients based on the age, and then based on age and fat thickness.

*1) Clustering based on age:* We adopt a heuristic approach to determine the age brackets for the subgroups. Starting from the youngest patient, we gradually increase the size of the first age group until the accuracy drops a lot. Once the first age group is determined, we repeat the above process for the next age groups, until we cluster all the patients. For male patients, this approach results in seven age brackets, namely [20, 30], [31, 40], [41, 49], [50, 55], [56, 60], [61, 69], and [70, 99], and an average accuracy of 75.2%. For female patients, this approach results in some age brackets for which the model always predicts higher water content under higher magnitudes.

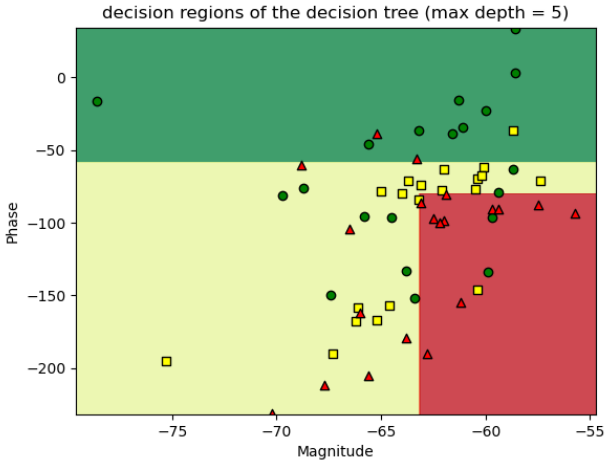


Fig. 11. Illustration of decision regions of an *undesirable* classifier for females patients with age between 35 and 45. It is undesirable because the red region (i.e., edema) is on the right to the yellow region (i.e., moderate edema).

TABLE II
SUMMARY OF MODEL ACCURACY.

| | | # of patients | accuracy | overall accuracy |
|---|---|---|---|---|
| Male | subgroup 1 | 28 | 78.6% | 71.9% |
| | subgroup 2 | 14 | 78.6% | |
| | subgroup 3 | 17 | 68.6% | |
| | subgroup 4 | 44 | 66.7% | |
| Female | subgroup 1 | 31 | 81.7% | 75.6% |
| | subgroup 2 | 23 | 60.9% | |
| | subgroup 3 | 34 | 84.3% | |
| | subgroup 4 | 13 | 64.1% | |

Such results violate the physics, because the signal should attenuate more when there is more lung water. Please see Fig. 11 for an illustration. Note that we did not exhaust all the possible clustering, which is practically impossible. But the phenomenon of predicting higher water content under higher magnitudes seems persistent in all the trials. As a result, we conclude that it is challenging to obtain interpretable models when clustering female patients based on the age only.

*2) Clustering based on age and fat thickness:* Since the fat thickness has been identified as an important feature, we cluster the patients based on both the age and the fat thickness. In particular, we divide the patients of the same gender into four subgroups by setting a threshold of the age and a threshold of the fat thickness. The median ages of male and female patients are 52 and 50, respectively. In our attempt to find the optimal thresholds of the age and the fat thickness, we choose the threshold of the age from $\{50, 55\}$ and the threshold of fat thickness from $\{6, 6.5, \ldots, 11.5, 12\}$. The optimal threshold is determined based on the average accuracy over the four subgroups.

We find that the optimal thresholds of the age are 50 for both male and female patients, and that the optimal thresholds of the fat thickness are 7.5mm and 11.5mm for male and female patients, respectively. Clustering based on age and fat thickness has two advantages over clustering based on age only. First, for male patients, we only need four subgroups, as

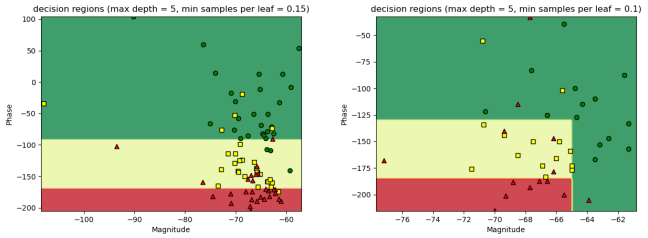


(a) age $\leq$ 50, fat thickness $<$ 7.5mm (b) age $\leq$ 50, fat thickness $\geq$ 7.5mm

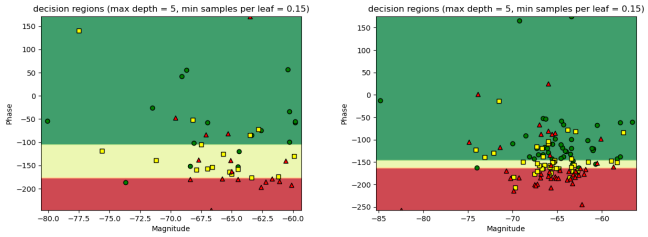


(c) age $>$ 50, fat thickness $<$ 7.5mm (d) age $>$ 50, fat thickness $\geq$ 7.5mm

Fig. 12. Decision regions of each subgroup of male patients. In all the subplots, the x-axis and y-axis are the magnitude and the phase of the S-parameters, and the green circles, yellow squares, and red triangles are the data samples representing normal water content (20%), moderate edema (40%), and edema (60%), respectively. The green, yellow, and red pixels indicate that the model classifies the corresponding samples as normal water content, moderate edema, and edema.

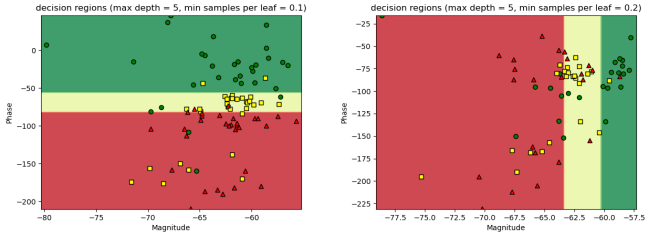


(a) age $\leq$ 50, fat thickness $<$ 11.5mm(b) age $\leq$ 50, fat thickness $\geq$ 11.5mm

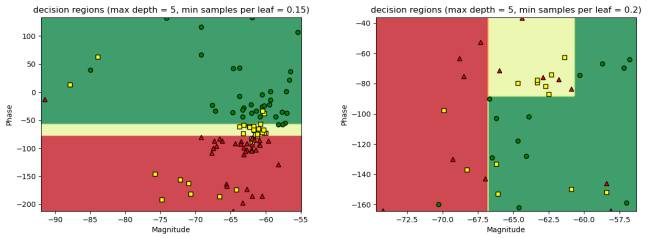


(c) age $>$ 50, fat thickness $<$ 11.5mm(d) age $>$ 50, fat thickness $\geq$ 11.5mm

Fig. 13. Decision regions of each subgroup of female patients.

opposed to seven in clustering based on age, to achieve similar average accuracy of 71.9%. For female patients, the predicted lung water content always decreases with the magnitude, which conforms to the physics. We summarize the results in Table II. The decision regions of the classifiers for male and female patients are shown in Fig. 12 and Fig. 13, respectively.

Compared to clustering based on the age only, clustering based on the age and the fat thickness is better, because it leads to fewer subgroups (i.e., four subgroups as oppose to seven) with negligible sacrifice in the accuracy. For each subgroup, the decision trees determine the lung water status based on the magnitude and the phase of the S-parameters, resulting in simple and interpretable decision rules.

### D. Model Interpretation

It is important to interpret the machine learning model [19]. For our study, we check if the model conforms with with the following expert knowledge:

- Our prior works suggest that the phase is the most important feature [23].
- According to electromagnetics, the magnitude of the signal decreases when there is more water in the lung.
- We apply the two chest patches, acting as the transmitter and the receiver, on the chest, as opposed to one on the chest and one on the back. Therefore, the chest circumference has limited impact on the signal strength.
- In clustering based on age and fat thickness, the threshold of the fat thickness is lower for male patients (7.5mm) compared to female (11.5mm). This makes sense because males have lower body fat percentages on average.

Our results are consistent with the expert knowledge mentioned above. The importance of the phase and the limited impact of the circumference are observed in our study on feature importance (see Fig. 12 and Fig. 13). The monotonic relationship between the magnitude and the lung water content is observed from the decision regions (see Fig. 12 and Fig. 13).

## V. Conclusion

In this paper, an AI-based wireless cardio-pulmonary stethoscope is developed for continuous non-invasive assessment of lung water status. The proposed AI-based CPS expands the capabilities of our previous wireless CPS to assessing lung water status (i.e., normal lung water content, moderate edema, and edema) of a diverse patient population, in addition to monitoring the change of lung water content. We use a large NIH database containing CT scan images of the lungs of a diverse population. Then an automatic workflow is proposed to convert these images to 3D lung objects in HFSS and obtain the S-parameters of the lungs at different water levels. This approach results in a database of a diverse patient population without expensive and time-consuming clinical trials. Using this database, we develop a personalized machine learning model to assess lung water status based on the patient attributes and S-parameter measurements. Our AI model adopts decision trees as the classifier for its superior accuracy and interpretability. Then we propose a "cluster-then-predict" approach, namely clustering the patients into subgroups and training a decision tree for each subgroup. This leads to even simpler and more interpretable decision rules with high accuracy. When the patients are clustered based on their ages, the resulting decision trees for the male patients perform well, but those for the female patients are hard to interpret. Therefore, the patients of each gender are clustered based on both their ages and fat thickness. The final decision trees for each cluster determine lung water status using S-parameters only, which are easy to interpret. Overall, our models achieve more than 70% accuracy over 103 male and 101 female patients of different ages (20 to 86) and body fat levels.

## References


[1] M. F. Iskander, N. Celik, R. Gagarin, G. C. Huang, and D. A. Bibb, "Microwave stethoscope for measuring cardio-pulmonary vital signs and lung water content," Dec. 27 2016, U.S. Patent 9526438.

[2] M. F. Iskander, T. B. Seto, R. R. Perron, E. Lim, and F. Qazi, "Cardio-pulmonary stethoscope: Clinical validation with heart failure and hemodialysis patients," *IEEE Transactions on Biomedical Engineering*, vol. 65, no. 5, pp. 1176–1180, 2017.

[3] M. F. Iskander and R. R. Perron, "Lung water content measurement system and calibration method," Dec. 8 2020, U.S. Patent 10856806 B2.

[4] ——, "Lung water content measurement system and calibration method," Jan. 11 2022, U.S. Patent 11219411.

[5] D. Bibb, R. R. Perron, G. C. Huang, and M. F. Iskander, "Development of a wireless monitoring system for microwave-based comprehensive vital sign measurement," *IEEE Antennas and Wireless Propagation Letters*, vol. 15, pp. 1249–1252, 2015.

[6] N. Celik, R. Gagarin, H.-s. Youn, and M. F. Iskander, "A noninvasive microwave sensor and signal processing technique for continuous monitoring of vital signs," *IEEE Antennas and Wireless Propagation Letters*, vol. 10, pp. 286–289, 2011.

[7] N. Celik, R. Gagarin, G. C. Huang, M. F. Iskander, and B. W. Berg, "Microwave stethoscope: Development and benchmarking of a vital signs sensor using computer-controlled phantoms and human studies," *IEEE transactions on Biomedical Engineering*, vol. 61, no. 8, pp. 2341–2349, 2013.

[8] M. Iskander and C. Durney, "Microwave methods of measuring changes in lung water," *Journal of Microwave Power*, vol. 18, no. 3, pp. 265–275, 1983.

[9] C. Leong, Y. Xiao, Z. Yun, and M. F. Iskander, "Non-invasive stethoscope for continuous assessment of lung water: Towards AI-based data augmentation and prediction," in *2022 IEEE International Symposium on Antennas and Propagation and North American Radio Science Meeting*, 2022.

[10] FCC, "Evaluating Compliance with FCC Guidelines for Human Exposure to Radiofrequency Electromagnetic Fields," June 2001, Washington, DC.

[11] K. Yan, X. Wang, L. Lu, and R. M. Summers, "DeepLesion: Automated mining of large-scale lesion annotations and universal lesion detection with deep learning," *Journal of Medical Imaging*, vol. 5, no. 3, p. 036501, 2018.

[12] P. C. Pedersen, C. C. Johnson, C. H. Durney, and D. G. Bragg, "Microwave reflection and transmission measurements for pulmonary diagnosis and monitoring," *IEEE Transactions on Biomedical Engineering*, vol. BME-25, no. 1, pp. 40–48, 1978.

[13] ANSYS HFSS. (Version 14.0), ANSYS Inc., https://www.ansys.com/products/electronics/ansys-hfss.

[14] C. Cortes and V. Vapnik, "Support-vector networks," *Machine learning*, vol. 20, no. 3, pp. 273–297, 1995.

[15] T. Hastie, R. Tibshirani, J. H. Friedman, and J. H. Friedman, *The elements of statistical learning: data mining, inference, and prediction*. Springer, 2009, vol. 2.

[16] T. K. Ho, "The random subspace method for constructing decision forests," *IEEE Transactions on Pattern Analysis and Machine Intelligence*, vol. 20, no. 8, pp. 832–844, 1998.

[17] I. Goodfellow, Y. Bengio, and A. Courville, *Deep learning*. MIT press, 2016.

[18] J. Goldberger, G. E. Hinton, S. Roweis, and R. R. Salakhutdinov, "Neighbourhood components analysis," *Advances in Neural Information Processing Systems*, vol. 17, 2004.
[19] C. Molnar, *Interpretable Machine Learning*, 2nd ed., 2022. [Online]. Available: https://christophm.github.io/interpretable-ml-book
[20] A. Fisher, C. Rudin, and F. Dominici, "All models are wrong, but many are useful: Learning a variable's importance by studying an entire class of prediction models simultaneously." *J. Mach. Learn. Res.*, vol. 20, no. 177, pp. 1–81, 2019.
[21] R. Soni and K. James Mathai, "An innovative "cluster-then-predict" approach for improved sentiment prediction," in *Advanced Computing and Communication Technologies*. Springer, 2016, pp. 131–140.
[22] J. Gálvez-Goicuría, J. Pagán, A. B. Gago-Veiga, J. M. Moya, and J. L. Ayala, "Cluster-then-classify methodology for the identification of pain episodes in chronic diseases," *IEEE Journal of Biomedical and Health Informatics*, vol. 26, no. 5, pp. 2339–2350, 2021.
[23] M. F. Iskander, R. Maini, C. H. Durney, and D. G. Bragg, "A microwave method for measuring changes in lung water content: Numerical simulation," *IEEE Transactions on Biomedical Engineering*, no. 12, pp. 797–804, 1981.